Geophys. J. Int. (2006) **167,** 838–844 doi: 10.1111/j.1365-246X.2006.03190.x

Multistation infrasonic observations of the Chilean earthquake of 2005 June 13

A. Le Pichon, P. Mialle, J. Guilbert and J. Vergoz

CEA/DASE/LDG, BP12, 91680 *Bruyères-le-Châtel, France. E-mail: alexis.le-pichon@cea.fr*

Accepted 2006 August 10. Received 2006 August 10; in original form 2006 February 23

SUMMARY

On 2005 June 13, a major earthquake (M7.8) occurred in the Tarapaca region (North Chile), within the region of high mountains. At large distances from the epicentre, this event produced coherent infrasonic waves detected by three infrasound stations that are part of the International Monitoring System. The observed azimuth variations and the long signal durations suggest that wide regions in the Andes Mountains radiated infrasonic waves. From these observations, the main sources' regions are reconstructed. Such an event recorded by multiple stations offers an unique opportunity to evaluate the relative contributions of the different source mechanisms involved in large earthquakes as well as to improve our understanding of the amplification of ground displacement caused by the topography. With a review of infrasound signals from past earthquakes, extended empirical scaling relations are derived. We show that beyond the seismic magnitude, both seismic source and topographic features also play a predominant role in the generation of infrasound.

Key words: atmosphere, earthquake, strong ground motion, waveform analysis, wave propagation.

1 INTRODUCTION

Large earthquakes are a well-known source of pressure waves. Acoustic-gravity waves from the sudden strong vertical ground displacements have been observed on microbarometers at distances of thousands kilometres from the origin (Donn & Posmentier 1964; Mikumo 1968). Distinct source mechanisms of pressure waves generation have been identified:

(i) pressure changes due to the vertical displacement of the seismic waves near the infrasound station; these receptions are associated in part with the instrumental response of the microbarometer to seismic waves (Kim *et al.* 2004; Yu *et al.* 2005),
(ii) the local conversion from seismic waves to the sound pressure near the epicentre area (Cook 1971; Olson *et al.* 2003; Takahashi *et al.* 1994), and
(iii) radiated pressure waves by the topography when seismic surface waves travel through mountainous regions (Young & Greene 1982; Mutschlecner & Whitaker 2005).

Some studies based on the recordings of one single station focused on the location of the infrasound source regions. They investigated the effects of both the directivity of the seismic source, and the configuration of the topography on the acoustic radiation (Le Pichon *et al.* 2003; Le Pichon et al. 2005a).

On 2005 June 13, a major earthquake occurred in the mountainous section of the Tarapaca Province (North Chile) (19.93°S–69.03°W at 22:44:33 UTC, M7.8, focal depth 117 km, USGS). The epicentre was located deep under the Andes mountain range, near Chile's border with Bolivia. At large distances from the epicentre, coherent infrasonic waves have been detected by three infrasound stations that are part of the International Monitoring System (IMS) (Hedlin *et al.* 2002). This earthquake, recorded by multiple stations at different ranges and azimuths from the epicentre, provides a unique opportunity to improve our understanding of the generation of acoustic waves produced by seismic wave-induced ground motion. This favourable setting allows:

(i) the validation of infrasonic celerity models and attenuation lows along multiple propagation paths,
(ii) a more complete reconstruction of the infrasound source regions compared to what could be obtained using one single station, and
(iii) a better knowledge of the different factors that influence the generation of infrasound.

In this paper, detailed analyses of these signals are first presented. Based on the infrasound measurements and 3-D ray-tracing simulations, enhanced localizations of infrasound source are calculated. Then, from the reconstructed radiating zones, we discuss the amplification of the ground displacement caused by the topography. Finally, wide-range estimates for infrasound observables are provided by extending existing empirical laws to a wide range of seismic magnitude.

Table 1. Name and location of the studied IMS infrasound stations.

Stations	Latitude	Longitude	Altitude (m)	Distance station/epicentre (km)
I08BO	16.21°S	68.45°W	4095	410
I09BR	14.64°S	48.02°W	1185	2300
I41PY	26.34°S	57.31°W	165	1420

Table 2. Main characteristics of the infrasound signals generated by the 2005 North Chile earthquake.

Stations	Duration (minutes)	Azimuth range (°)	Max. amplitude (Pa)	Max. period (s)
I08BO	26	184–227	1.41	10
I09BR	52	240–265	0.11	3
I41PY	17	293–304	0.18	1

2 INFRASOUND MEASUREMENTS

The IMS infrasound stations I08O-Bolivia, I09BR-Brazilia, and I41PA-Paraguay (Table 1) recorded large coherent infrasonic waves produced by the Chilean earthquake of 2005 June 13 (Fig. 1). In this study, we focus on the distant generation of pressure waves radiated by extended source regions. The wave parameters are calculated with the *progressive multichannel correlation* method (PMCC) (Cansi 1995). With a sampling rate of 20 Hz, the expected numerical resolution at 0.5 Hz is of the order of 2° for the azimuth and 5 m s^{-1} for the horizontal trace velocity. The main characteristics of the detected signals are summarized in Table 2. At I08BO, between 22:45 and 22:52 UTC, large coherent signals are detected with a trace velocity greater than 3 km s^{-1}, which is consistent with the propagation of seismic waves. These arrivals are primarily a manifestation of the seismic response of the microbarometer. The PMCC analysis displays clear backazimuth trends of over 11°, 25°, 43° at I41PY, I09BR and I08B0, respectively, while the trace velocity ranges from 0.34 to 0.37 km s^{-1}. The period at the maximum of amplitude is around 10 s with a maximum peak-to-peak amplitude of ∼1.4 Pa at I08BO. The long signal duration and the large azimuth variations suggest that wide regions acted as sources of infrasound. They are explained by an extended radiation area along the fault rupture, and the increase of the effective infrasound source region when seismic surface waves travel from the fault rupture through regions of high mountains where radiation occurs.

3 LOCALIZATION OF INFRASOUND SOURCES REGION

3.1 Methodology

From these observations, the main source regions of infrasound are reconstructed. The input parameters of the location procedure include the azimuths and arrival times measured independently by each station, the origin time and coordinates of the epicentre. As discussed in Section 4, a joint inversion for the source area using data from all three stations simultaneously is not appropriate due to the pronounced directivity of the radiation pattern. The velocity models used describe the propagation of the seismic surface waves and the propagation of infrasound in the direction of each station. Infrasonic waves propagate in the atmosphere over very large distances in the waveguide formed by the atmosphere and its temperature gradients. Ducting is especially efficient in the ground to stratosphere and thermosphere waveguides. It can be reinforced or reduced by the high-altitude winds (Garcés *et al.* 1998). The long-range infrasound propagation is simulated using the

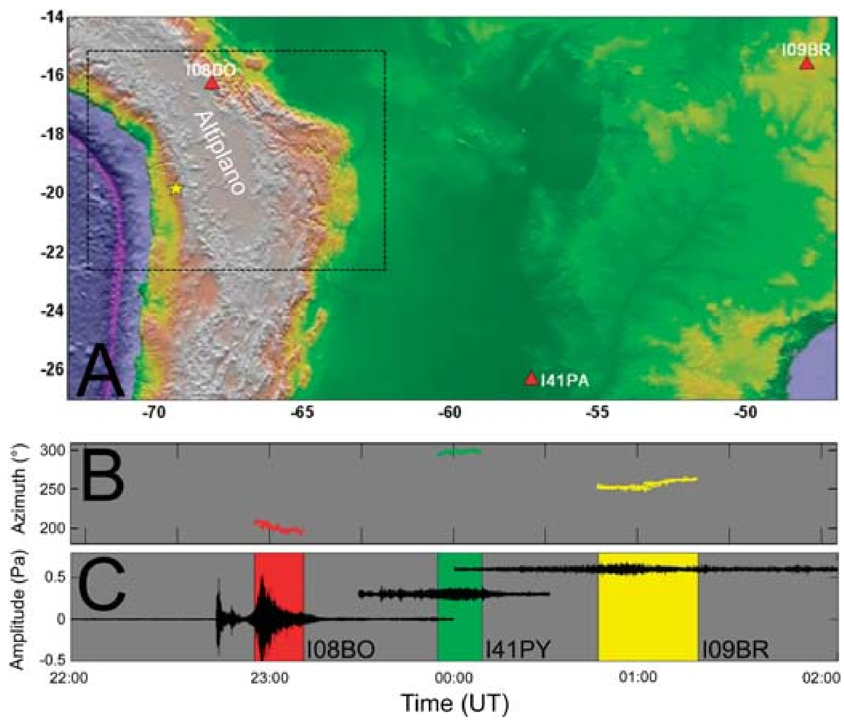

Figure 1. Topography of the region of interest. (a) The spatial grid used for the simulations is delimited by the black rectangle. The atmospheric conditions of 2005 June 13 are described over a grid of resolution 0.5°, ranging from latitude 15° to 23°S, longitude 62° to 72°W, altitude 0 to 180 km and time between 22:00 and 02:00 UTC. The yellow star and the red triangle indicate the epicentre and the location of the three infrasound station, respectively. (b) Backazimuth from North (deg) calculated by PMCC. (c) Atmospheric pressure fluctuations recorded at the central elements filtered between 0.1 and 2 Hz.

WASP-3D ray theory-based method which account for the topography and the spatiotemporal variations of the horizontal wind terms along the ray paths. The equations describe the evolution of the ray canonical variables (slowness vector, position and propagation time) and are numerically solved in spherical coordinates (Dessa *et al.* 2005). Assuming limited pressure perturbations, the motion of the atmospheric medium is ruled by the linearized hydrodynamic equations for a compressible fluid. This implies that the signal wavelengths are smaller than those of atmospheric property variations. Considering both the dominant period of the signals (Table 2) and the used spatial resolution of the atmospheric specifications, the high-frequency asymptotic approximation is appropriate. A paraxial approach for the amplitude computation is used. Small perturbations of the slowness vector and position around a central ray of reference enable to estimate in three dimensions the evolution of the cross-section of a ray tube, hence giving the local amplitude of the signal. The atmospheric absorption is integrated using attenuation coefficients varying with altitude, frequency of the propagating wave and atmospheric parameters (gas composition, density, pressure, temperature and humidity) (Bass & Sutherland 2004). The wave attenuation is computed according to the frequency at the maximum of amplitude of the phase-aligned signals at each station. The atmospheric conditions of 2005 June 13 are described by the sound velocity and wind speed profiles provided by the time-varying ground-to-space (G2S) atmospheric model (Drob *et al.* 2003). We first define a spatial grid whose extension is adjusted by uncertainties in the propagation model (± 40 m s^{-1} around a mean celerity—horizontal propagation range divided by traveltime—of 290 m s^{-1}, Fig. 2). Then, applying a shooting procedure, 80 rays are launched from each cell of the grid at the altitude of the ground level in the direction of each station. Slowness values are derived from the measured trace velocity (between 2.6 to 3.0 s km^{-1}). Finally, the azimuthal deviation, celerity values and attenuation are calculated for each ray trajectory.

3.2 Propagation models

As pointed out by Drob *et al.* (2003), natural changes in the background atmospheric state variables greatly influence the propagation of infrasonic signals. A study of the statistical performance measures of the HWM-93 empirical model highlighted systematic errors in the zonal wind field from 35 to 120 km ranging from 20 to 50 m s^{-1} (Drob & Picone 2000). These climatological biases have been confirmed using infrasonic ground-truth events. A continuous monitoring of infrasound signals from active volcanoes has been proposed as a remote sensing method of the upper atmosphere (Le Pichon et al. 2005b). The final results of the developed inversion procedure showed that the mesospheric wind jet in the G2S wind model is underestimated by at least 20 m s^{-1} throughout the year, and the strong wind region in the stratosphere should be extended to the lower thermosphere. Part of the random errors in the wind estimates is also attributable to the stochastic variability of the medium filtered out from the models—transient wave phenomena such as large-scale gravity waves and propagating planetary waves are irresolvable by today's observationally based global atmospheric specification systems. These errors were found to be large enough to result in inaccurate estimates ducting heights, as well as traveltimes, and possibly source location estimates. In order to improve phase identification and localization, perturbed realizations of atmospheric conditions are incorporated into our modelling. We introduce a Gaussian correction factor to the prevailing zonal wind component, centred at 80 km with a half-width of 30 km, of amplitude randomly distributed between 0 and 20 m s^{-1}. Following the nomenclature defined by Brown *et al.* (2002), estimates of celerity, azimuthal deviation and attenuation are calculated within each ray class (i.e. Iw—tropospheric, *Is*—stratospheric or *It*-thermospheric phases). For that, we consider the ground reception of rays if bounces are contained within a circle of radius equal to one-tenth of the propagation range around each station before averaging the properties of the selected rays. In case of multiple arrivals, and in order to avoid mixing properties between different ray classes, phases with the lowest attenuation are selected.

3.3 Seismic source

In order to check the consistency of regions radiating infrasound with areas of strong ground motion, we use the slip patches model developed by Vallée & Bouchon (2004) which looks for the

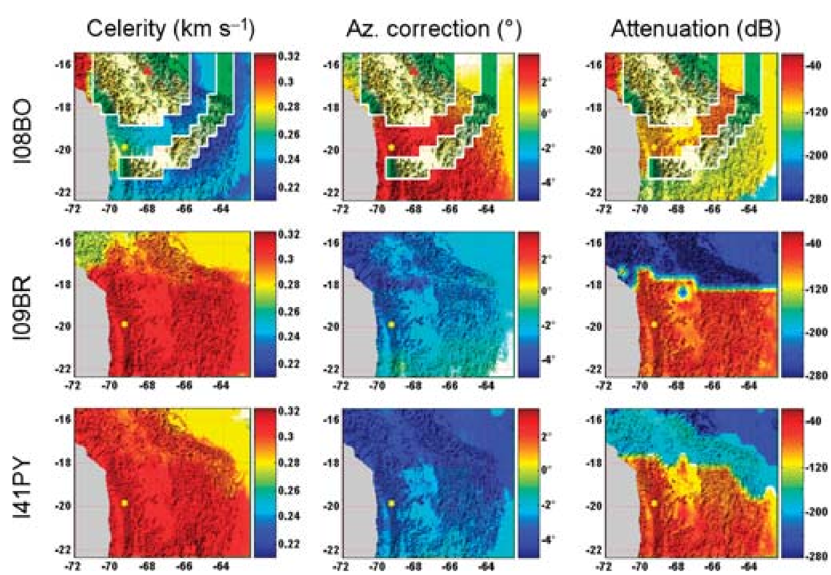

Figure 2. Range dependent propagation models for the Chilean earthquake of 2005 June 13. From left to right: Colour refers to the celerity, azimuthal corrections, and attenuation. Regions without colour are the surface ocean (no possible source) and shadow zones where no detectable energy at I08BO is predicted by the ray theory for sources contained within these regions.

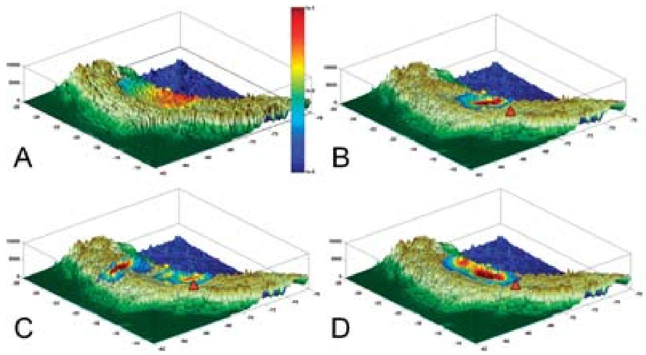

Figure 3. Location distribution of the distant infrasound source regions. (a) Mean-square root of the maximum ground velocity (in m s^{-1}) of the vertical and horizontal components for periods greater than 20 s (normalized amplitude). (b, c, d) Reconstructed source regions for stations I08BO, I09BR and I41PY, respectively. Colours are normalized to the maximum number of localizations per unit of surface derived from the infrasound measurements (linear scale from blue to red).

simplest extended elliptic source model able to explain the teleseismic seismograms of the 2005 June 13 Chile earthquake. The first- and second-order characteristics of the event (location, depth, duration, focal mechanism, and refined kinematic parameters such as spatial slip distribution on the fault and rupture velocity) are calculated from teleseismic *P* and *SH* body waves. Then, from the resulting extended source model, low-frequency synthetic seismograms (period lower than 10 s) are computed on a grid in the vicinity of the epicentre using the discrete wavenumber method and a 1-D regional crust model (Bouchon 1981). Finally, the rms of the maximum velocity of the vertical and horizontal components of the surface waves is used to reconstruct the areas of strong ground motion. This intermediate-depth earthquake occurred at a depth of 117 km. Rupture propagates bilaterally (on a little less than 100 km) and downdip, which is consistent with studies of Yagi (2005) and Yamanaka (2005). The maximum slip on the fault is evaluated to about 6 m. The calculated near field ground velocities show a maximum area around the hypocentre (Fig. 3a).

3.4 Results

Fig. 2 presents the range dependent propagation models derived for each station. The component of the wind transverse to the propagation direction deflects the rays from the original launch azimuth. Depending on the station and the location of the source, azimuthal corrections range from $-4°$ to $3°$. Celerity values are consistent with the propagation tables defined by Brown *et al.* (2002): 0.23–0.28 km s^{-1} and 0.28–0.31 km s^{-1} for *It* and *Is* phases, respectively. As expected, propagation models for the two farthest stations are relatively straightforward with weak variations in celerity and azimuthal corrections. As the propagation range decreases, results are more widely distributed. Because rays from the epicentre area propagate almost in a direction perpendicular to the eastward-dominant zonal winds in the direction of I08BO, the increase of the effective sound speed is not strong enough to favour stratospheric returns. Thus, most of the rays return back to the ground after being refracted in the thermosphere (Fig. 3b). The relative low-frequency content of the detected signals is compatible with this phase identification. Around I08BO, well-defined shadow zones decrease the area of investigation as ray theory predicts no detectable energy for sources contained within these regions. Beyond several ray bounces, the effect of the shadow zone decreases with distance as rays within each waveguide start to overlap. With the defined criteria for the ground reception of infrasound energy, shadow zone disappears for propagation ranges larger than ∼1000 km, and the propagation models become uniformly distributed over the source regions of interest. In the direction of I09BR, the prevailing zonal winds allow the formation of a stratospheric duct below ∼40 km height for sources located below latitude 18°S (Fig. 3c). At higher latitudes, one single thermospheric waveguide with negligible amplitude is predicted. In the direction of I41PY, three different ray classes are identified: *Is*, *It* converted into *Is* and *It* from south to north (Fig. 3d). Considering the strong attenuation for *It* phases originating above 18°S, sources of coherent waves detected at I09BR and I41PY are likely located in the southern part of the grid. Enhanced localizations are then computed using celerity estimates and azimuth measurements corrected by azimuthal deviation estimates. Applying a grid search procedure over the investigated source region (zone delimited in Fig. 1), the final solution minimizes residuals between measurements and simulations for both wind-corrected azimuths and arrival times for each individual station. Taking into account the propagation variability due to atmospheric uncertainties and errors in the measurements, a maximum location error of 50 km is estimated.

The Andes run in two great parallel ranges culminating at ∼6000 m. The western range (Cordillera Occidental) runs along the Peruvian and Chilean borders. The eastern range (Cordillera Oriental) is a broad and towering system of mountains stretching from Peru to Argentina. The Altiplano, a sediment-filled depression about 4000 m above sea level, which is approximately 1000 km long from North to South and 150 km wide, lies between the Occidental and Oriental ranges (Fig. 1). The reconstructed source regions fall into line with these ranges. More precisely, the radiating zone extends from the Central Cordillera near Argentina's border with Bolivia to the Occidental Cordillera about 200 km to the north of the epicentre. Infrasonic waves from mountainous regions along the North Chile's border have been recorded by all stations. A second region located to the south of the Altiplano also efficiently radiated energy, although infrasound signals have been only detected by the farthest station I09BR.

4 EMPIRICAL RELATIONS BETWEEN INFRASOUND OBSERVABLES AND SEISMIC MAGNITUDE

As demonstrated by previous works and confirmed in the present study (Le Pichon *et al.* 2003; Madshus *et al.* 2005), the ground coupled infrasonic waves generated during large earthquakes provide an image of the interaction between the surface wave radiation pattern and the topography in the fault rupture region. Some characteristics of the measured infrasound signals provide information relative to the seismic magnitude, but also the seismic source mechanism and its interaction with high mountain ranges. We focus here on the relation between infrasound observables such as amplitude and duration, and the seismic magnitude. The data used include the 2005 Chilean event as well as some great earthquakes.

4.1 Magnitude–amplitude relation

As shown by Mutschlecner & Whitaker (2005), the amplitude of infrasound signals from earthquakes is affected by: (i) the distance from the source by roughly a cylindrical fall-off rate as a result of ducted propagating waves and (ii) the stratospheric wind direction.

Table 3. Main characteristics of infrasound signals generated by 12 large earthquakes ($M_S > 6.7$, (USGS)).

No.	Earthquakes	M_S	Stations	Distance station/ epicentre (km)	Duration (minutes)	Max. amplitude (Pa)
1	2005 June 13	7.4	I08BO	410	26	1.41
2	Chile		I09BR	2300	52	0.11
3			I41PY	1420	17	0.18
4	2003 May 26 Japan (Lee *et al.* 2004)	7.0	CHNAR	1250	40	0.15
5	2001 November 14	8.0	I34MN	1850	70	1.65
6	China (Lee *et al.* 2004)		CHNAR	3230	60	0.20
7	2001 June 23 Peru (Le Pichon *et al.* 2002)	8.2	I08BO	530	50	2.50
8	2002 November 3	8.5	I10CA	3360	120	0.15
9	Alaska (Olson *et al.* 2003)		I53US	130	46	12.10
10	2005 April 10 Sumatra (Garcés *et al.* 2005) (Le Pichon et al. 2005)	8.4	I52GB	3070	75	0.55
11	2005 March 28 Sumatra (Garcés *et al.* 2005) (Le Pichon et al. 2005)	6.7	I52GB	2940	15	0.05
12	2005 October 8, Pakistan	7.6	I31KZ	2170	56	0.27

They proposed a scaling relation which accounts for these two effects has been proposed:

$$A_n = A_0 \left(\frac{R}{R_n}\right)^s 10^{-kV_d}, \tag{1}$$

where A_n is the zero-wind amplitude normalized to standard distance R_n set to 1000 km, A_0 is the zero-to-peak observed amplitude (in μbar), R is the source-to-receiver distance (in km), V_d is the component of the stratospheric wind at 50 km in the direction of propagation (in m s^{-1}), s and k are empirical constants which are taken as 1.45 and 0.018 s m^{-1}, respectively. Mutschlecner & Whitaker (2005) suggested that the infrasound amplitude is related to the seismic magnitude which, in turn, drives the infrasound generation. They proposed an other relation derived from the observation of 31 earthquakes (with magnitudes lower than 7.3) detected by arrays of microphones operated by the Los Alamos National Laboratory:

$$\log(A_n) = 0.55\, M_L - 4.0, \tag{2}$$

Shallow earthquakes (depth lower than 30 km) generate large surface waves compared to similar earthquakes at larger depth (Herak *et al.* 2001). As demonstrated by Le Pichon *et al.* (2003) and Guilbert *et al.* (2003), the area of ground coupling air waves is clearly correlated with the surface wave radiation pattern. The surface wave magnitude M_S measured for 20 s period Rayleigh waves would be then more relevant to correlate infrasound observables with the seismic energy radiated by the earthquake. Furthermore, due to its definition, the M_L magnitude is not appropriate for magnitude greater than 5.5 (Utsu 2003). Using the following empirical relation between M_S and M_L given by Utsu (2003),

$$M_S = 1.27 \times (M_L - 1) - 0.016 \times M_L^2, \tag{3}$$

the magnitude–amplitude relation proposed by Mutschlecner & Whitaker (2005) has been corrected. Then, we added the measurements of seven earthquakes of larger magnitude (Table 3), sometimes recorded by multiple stations. Fig. 4(a) shows the relation between the logarithm of the normalized amplitudes as defined by

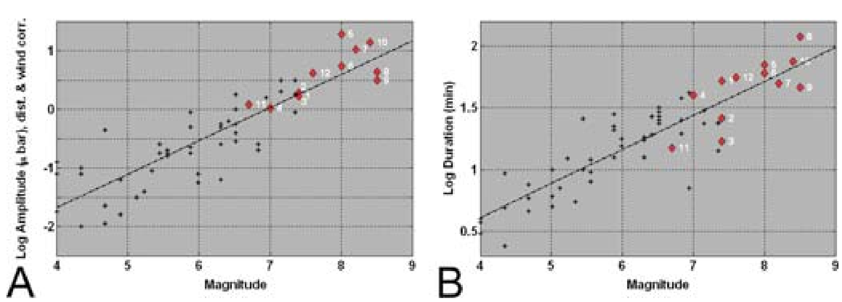

Figure 4. Empirical scaling relations. (a, b) Relation between the normalized amplitude and duration of infrasound signals versus seismic M_S magnitude. Black dots: Measurements of 31 earthquakes detected by arrays of microphones operated the Los Alamos National Laboratory. Red dots: Measurements from 7 earthquakes of magnitude larger than M_S 6.7. Numbers refer to the event list described in Table 3.

eq. (1) and the seismic magnitude. Using a standard least-squares procedure, a linear scaling relationship is derived:

$$\log(A_n) = 0.57M_S - 3.95. \quad (4)$$

Although there is scattering in our scaling relation, the linear fit is acceptable for large magnitudes and is furthermore in close agreement with eq. (2). This analysis confirms that the normalized amplitude of infrasound signals corrected for the propagation is well correlated to the ground motion strength for a wide range of magnitude.

4.2 Magnitude–duration relation

Fig. 4(b) compares the duration of the same measurements to the seismic magnitude. Although the scattering is large (in a range of one order of magnitude), the duration also correlates with magnitude:

$$\log(Dur) = 0.28\, M_S - 0.50, \quad (5)$$

where *Dur* is the duration of the detected coherent infrasonic waves (in minutes). This relation is consistent with the one proposed by Mutschlecner & Whitaker (2005) using the M_L magnitude. It confirms that the duration of the infrasound signals is primarily driven by the seismic magnitude (including the rupture length and focal depth). In the case of the North Chile earthquake, the duration of the signals induced by the regional excitation of the topography differs significantly from one station to another. It suggests that the measured infrasound signals produced by the excitation of topography are also sensitive to the directivity of the radiating area at local and regional distances.

5 DISCUSSION

The reconstructed source regions confirm that most of the energy is radiated by the vibration of land masses near the epicentre. All stations detected a predominant radiating zone near the epicentre, which is consistent with the predicted areas of strong ground motion. No clear signal originates from the Altiplano. Southern high mountain ranges, even far from the epicentre, also generated infrasound. The Central Cordillera culminating at altitudes greater than 5000 m efficiently produced infrasound in the direction of I09BR, although the predicted seismic movement is low in this region. These results suggest an amplification of the ground displacement caused by the topography surrounding the Altiplano. Such site effect could not be predicted since the topography is not considered in our seismic source modelling.

The physics for generation of overpressure above a moving surface was given by Rayleigh (1945) and involves an integration of the acceleration (or ground velocity) of the surface over the area in motion. As a result, the infrasound source regions involve the propagation of seismic surface waves from the epicentre through succession of ridges. Mutschlecner & Whitaker (2005) proposed that the signal duration primarily depends on the radius at which the peak vertical acceleration reaches a limited value for effective sound generation. It appears that the duration cannot simply be related to the magnitude. Considering the topography as a succession of adjacent strip-line sources, mountain ranges radiate energy essentially simultaneously with a pronounced directivity and may generate infrasound arrivals with different azimuths (Le Pichon *et al.* 2003). We suggest that the amount of energy radiated in the direction of the receiver and the duration of the signals also depend on the orientation of the highest mountain ranges around the station. More detailed analyses of durations will require corrections for the effects of the seismic source parametrization (such as depth, source mechanism) and topographic features (extension, geographic situation).

6 CONCLUDING REMARKS

The large Chilean earthquake that occurred in the Andes Mountains on 2005 June 13 generated infrasonic waves that were observed beyond 2000 km by multiple IMS stations. Propagation tables derived from 3-D ray-tracing simulations predict a dominant stratospheric waveguide for I09BR and I41PY, and ducted thermospheric waves for I08BO. The reconstructed source regions extend over ∼800 km from the Central Cordillera to the Occidental Cordillera. The spatial extent of the radiating zones differs from one station to another, which confirms the influence of both shadow zone effects for nearby station, and the directivity of the radiation. One predominant radiating zone is located near the epicentre which is consistent with predicted areas of strong ground motion. A second southern source region reconstructed along the Central Cordillera indicates possible amplification of the ground motion induced by site effects. The close agreement between the magnitude–amplitude relations derived from different data set confirms the strong influence of the ground motion. A larger scattering is found in the duration–magnitude relation, more specifically for magnitudes larger that 7. We suggest the signal duration may not only be restricted to the seismic magnitude. The seismic source mechanism and the geographic situation of the mountain ranges relative to the areas of strong ground motion may also play a predominant role in the generation of infrasound. Multiple stations infrasonic observations will probably occur more frequently in the future because of the increasing number of IMS stations being deployed. Future use of the IMS could rapidly expand the database of detections and correspondingly enhance our understanding of signal characteristics using earthquake parametrizations beyond magnitude. By combining seismic and infrasonic methods, more studies like the one presented here are valuable for the analysis of the remote effects of earthquakes. The modelling of the source generation and acoustic propagation in a complex medium should be pursued. In particular, the use of surface motion data in extended region would be valuable and could help to explain duration characteristics. With a better knowledge of the different factors that influence the generation of infrasound, these studies could lead to a rapid determination of the regions where the seismic movements are the largest, more especially when there is a lack of surface motion instrumentation.

ACKNOWLEDGMENTS

The data used in this article were provided by the IDC in Vienna. The authors are grateful to Dr Y. Cansi and N. Brachet for their interest in this study and for the helpful discussions we had during the completion of this work. We would like also to thanks D. Drob for providing us the NRL-G2S atmospheric specifications, and the NASA Goddard Space Flight Center, Global Modeling and Assimilation Office (GSFC-GMAO), NOAA National Centers for Environmental Prediction (NCEP) for providing the NWP data that went into the NRL-G2S atmospheric specifications.

REFERENCES

Alcoverro, B., Martysevich, P. & Starovoit, Y., 2005. Mechanical sensitivity of microbarometers MB2000 (DASE, France) and Chaparral 5 (USA) to vertical and horizontal ground motion, *Inframatics,* **9,** March 2005, 1–10, http://www.inframatics.org.

Bouchon, M., 1981. A simple method to calculate Greens functions for elastic layered media, *Bull. seism. Soc. Am.,* **71,** 959–971.

Brown, D.J., Katz, C.N., Le Bras, R., Flanagan, M.P., Wang, J. & Gault, A.K., 2002. Infrasonic signal detection and source location at the Prototype Data Centre, *Pure appl. Geophys.,* **159,** 1081–1125.

Cansi, Y., 1995. An automatic seismic event processing for detection and location: the PMCC method, *Geophys. Res. Lett.,* **22,** 1021–1024.

Cook, R.K., 1971. Infrasound radiated during the Montana earthquake of 1959 August 18, *Geophys. J. R. astr. Soc.,* **26,** 191–198.

Dessa, J.X., Virieux, J. & Lambotte, S., 2005. Infrasound modeling in a spherical heterogeneous atmosphere, *Geophys. Res. Lett.,* **32,** doi:10.1029/2005GL022867.

Donn, W.L. & Posmentier, E.S., 1964. Ground-coupled air waves from the great Alaskan earthquake, *J. geophys. Res.,* **69,** 5357–5361.

Drob, D.P. & Picone, J.M., 2000. Statistical performance measures of the HWM-93 and MSISE-90 empirical atmospheric models and the relation to infrasonic CTBT monitoring, 22nd Annual Seismic Research Symposium: Planning for Verification of an Compliance with the Comprehensive Nuclear-Test-Ban Treaty New Orleans, Louisiana, USA, 8p.

Drob, D.P., Picone, J.M. & Garcés, M.A., 2003. The global morphology of infrasound propagation, *J. geophys. Res.,* **108,** doi:10.1029/2002JD003307.

Garcés, M., Hansen, R. & Lindquist, K., 1998. Traveltimes for infrasonic waves propagating in a stratified atmosphere, *Geophys. J. Int.,* **135,** doi:10.1046/j.1365-246X.1998.00618.x.

Garcés, M., Caron, P., Hetzer, C., Le Pichon, A., Bass, H., Drob, D. & Bhattacharyya, J., 2005. Deep infrasound from the Sumatra earthquake and tsunami, *EOS, Trans. Am. geophys. Un.,* **86**(35).

Guilbert, J., Le Pichon, A., Alcoverro, B., Vallée, M. & Ulziibat, M., 2003, The ground-coupled air waves generated by the Kokoxili earthquake, 14th Nov. 2001 ($M_{\mathrm{w}} = 7.8$): an example of direct simulation and a rapid constraint on seismic source, *Geophysical Research Abstracts,* **5,** 06376, EGS-AGU-EUG, Nice, France.

Hedlin, M., Garcés, M., Bass, H., Hayward, C., Herrin, G., Olson, J. & Wilson, C., 2002. Listening to the secret sounds of earth's atmosphere, *EOS, Trans. Am. geophys. Un.,* **83,** 564–565.

Herak, M., Panza, G.F. & Costa, G., 2001. Theoretical and observed depth correction for Ms, *Pure appl. Geophys.,* **158,** 1517–1530.

Kim, T.S., Hayward, C. & Stump, B., 2004. Local infrasound signals from the Tokachi-Oki earthquake, *Geophys. Res. Lett.,* doi:10.1029/2004GL021178.

Lee, H.I., Che, I.Y. & Le Pichon, A., 2004. Infrasound network in Korea and observations of some interesting infrasonic events, paper presented at Infrasound Technology Workshop, Geoscience Australia, Hobart, Tasmania.

Le Pichon, A., Guilbert, J., Vallée, M., Dessa, J.X. & Ulziibat, M., 2002. Ground-coupled air waves and diffracted infrasounds from the Arequipa earthquake of June 23, 2001, *Geophys. Res. Lett.,* doi:1029/2002GL015052.

Le Pichon, A., Guilbert, J., Vallée, M., Dessa, J.X. & Ulziibat, M., 2003, Infrasonic imaging of the Kunlun Mountains during the great 2001 China earthquake, *Geophys. Res. Lett.,* doi:10.1029/2003GL017581.

Le Pichon, A., Herry, P., Mialle, P., Vergoz, J., Brachet, N., Garcés, M., Drob, D. & Ceranna, L., 2005a. Infrasound associated with 2004–2005 large Sumatra earthquakes and tsunami, *Geophys. Res. Lett.,* **32,** doi:10.1029/2005GL023893.

Le Pichon, A., Blanc, E. & Drob, D.P., 2005b. How can infrasound listen to high-altitude winds?, *J. geophys. Res.,* **110,** doi:10.1029/2005JD006020.

Madshus, C., Løvholt, F., Kaynia, A., Hole, L.R., Attenborough, K. & Taherzadeh, S., 2005. Air-ground interaction in long range propagation of low frequency sound and vibration-field tests and model verification, *Appl. Acoust.,* **66,** 553–578.

Mikumo, T., 1968. Atmospheric pressure waves and tectonic deformation associated with the Alaskan earthquake of March 28, 1964, *J. geophys. Res.,* **73,** 2009–2025.

Mutschlecner, J.P. & Whitaker, R.W., 2005. Infrasound from earthquakes, *J. geophys., Res.,* **110,** doi:10.1029/2004JD005067.

Olson, J.V., Wilson, C.R. & Hansen, R., 2003. Infrasound associated with the 2002 Denali fault earthquake, Alaska, *Geophys. Res. Lett.,* **30,** doi:10.1029/2003GL018568.

Rayleigh, J.W., 1945. *The Theory of Sound,* **Vol. 2,** 2nd edn, 1896, reprinted from Dover, NY.

Starovoit, Yu. O. & Martysevich, P.N., 2005. Different observed mechanisms of correlation between seismic and pressure signals, *Inframatics* **09,** 11–16.http://www.inframatics.org.

Sutherland, L.C & Bass, H.E., 2004. Atmospheric absorption in the atmosphere up to 160 km, *J. Acoust. Soc. Am.,* **115,** 1012–1032.

Takahashi, Y., Koyama, Y. & Isei, T., 1994. In situ measured infrasound at Sapporo associated with an earthquake occurring offshore in southwest Hokkaido on July 12, 1993, *J. Acoust. Soc. Jpn.,* **15,** 409–411.

USGS, Earthquake Hazards Program, http://earthquake.usgs.gov.

Utsu, T., 2003. *Relationships between Magnitude Scales*, International Handbook of Earthquake Engineering Seismology, pp. 733–746, Academic Press, Elsevier Science, Amsterdam.

Vallée, M. & Bouchon, M., 2004. Imaging coseismic rupture in far field by slip patches, *Geophys. J. Int.,* **156,** 615–630.

Virieux, J., Garnier, N., Blanc, E. & Dessa, J.X., 2004. Paraxial raytracing for atmospheric wave propagation, *Geophys. Res. Lett.,* **31,** doi:10.1029/2004GL020514.

Yagi, Y., 2005. Preliminary results of rupture process for Chile earthquake, Environmental Sciences, University of Tsukuba, http://www.geo.tsukuba.ac.jp/press˙HP/yagi/EQ/2005Chile.

Yamanaka, Y., 2005. EIC Seismological Note No.165 for Tarapaca, Chile earthquake, ERI (Univ. of Tokyo), http://www.eri.u-tokyo.ac.jp/sanchu/Seismo˙Note/2005/EIC165e.html.

Young, J.M. & Greene, G.E., 1982. Anomalous infrasound generated by the Alaskan earthquake of 28 March 1964, *J. acoust. Soc. Am.,* **71,** 334–339.